

Microscopic origin of temperature-dependent magnetism in spin-orbit-coupled transition metal compounds

Ying Li,^{1,*} Ram Seshadri,² Stephen D. Wilson,² Anthony K. Cheetham,^{3,4} and Roser Valenti^{5,†}

¹MOE Key Laboratory for Nonequilibrium Synthesis and Modulation of Condensed Matter, School of Physics, Xi'an Jiaotong University, Xi'an 710049, China

²Materials Department, University of California, Santa Barbara, CA 93106, USA

³Materials Research Laboratory, University of California, Santa Barbara, CA 93106, USA

⁴Department of Materials Science and Engineering, National University of Singapore, Singapore 117575

⁵Institut für Theoretische Physik, Goethe-Universität Frankfurt, Max-von-Laue-Strasse 1, 60438 Frankfurt am Main, Germany

(Dated: August 5, 2024)

A few $4d$ and $5d$ transition metal compounds with various electron fillings were recently found to exhibit magnetic susceptibilities χ and magnetic moments that deviate from the well-established Kotani model. This model has been considered for decades to be the canonical expression to describe the temperature dependence of magnetism in systems with non-negligible spin-orbit coupling effects. In this work, we uncover the origin of such discrepancies and determine the applicability and limitations of the Kotani model by calculating the temperature dependence of the magnetic moments of a series of $4d$ (Ru-based) and $5d$ (W-based) systems at different electron fillings. For this purpose, we perform exact diagonalization of *ab initio*-derived relativistic multi-orbital Hubbard models on finite clusters and compute their magnetic susceptibilities. Comparison with experimentally measured magnetic properties indicates that contributions such as a temperature independent χ_0 background, crystal field effects, Coulomb and Hund's couplings, and intersite interactions – not included in the Kotani model – are specially crucial to correctly describe the temperature dependence of χ and magnetic moments at various electron fillings in these systems. Based on our results, we propose a generalized approach beyond the Kotani model to accurately describe their magnetism.

Introduction.– The magnetism in spin-orbit coupled transition-metal-based compounds has been at the focus of intensive studies in recent years, not only due to their relevance for such phenomena as frustrated magnetism [1–5], Kitaev spin liquid phases [6–16], fractionalized excitations [3, 4, 17–19], or multipolar physics [20–24], but also for their role in, for instance, $4d$ and $5d$ hybrid halides, which are being discussed as relevant materials for optoelectronic purposes [25–29]. Due to the presence of spin-orbit coupling, the usual Curie-Weiss formula to explain the temperature-dependent susceptibility in these systems does not apply. To overcome this problem Kotani [30] proposed a temperature-dependent expression for magnetic moments [see Fig. 1 (a)], which successfully explains the behavior of the magnetic susceptibility in a few $4d$ and $5d$ systems. Some examples are ruthenium halides with perovskite-related structures such as A_2RuX_6 ($A = K, Cs, Rb$; $X = Cl, Br$) [31–33], and a few cases of Ru-based hybrid halides [34, 35]. In some other examples, including Ru-based hybrid halides $MA_2NaRuCl_6$ ($MA = CH_3NH_3$), $MA_3Ru_2Br_9$, and vacancy-ordered double perovskites A_2WCl_6 ($A = Cs, Rb, MA$) [36–38], the temperature-dependent magnetic susceptibility deviates strongly from

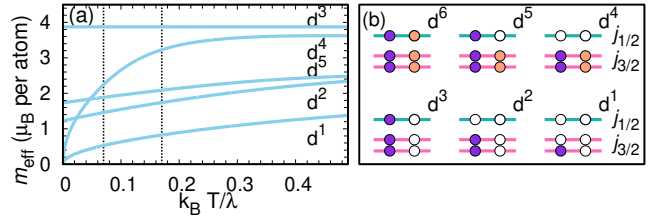


FIG. 1. (a) Kotani plot of m_{eff} for various fillings of t_{2g} orbitals. The dotted vertical lines at $k_B T / \lambda \sim 0.07$ and 0.17 eV indicate $T = 300$ K when $\lambda = 0.15$ eV ($4d$) and 0.37 eV ($5d$), respectively. (b) Schematic ground state diagrams for each filling in the relativistic $j_{1/2}$ and $j_{3/2}$ basis.

the Kotani prediction, challenging this well-established model for spin-orbit-coupled transition-metal complexes.

We recently considered extensions of Kotani's expression to describe the magnetism in a few cases of spin-orbit-coupled magnets, such as the iridium and ruthenium-based d^5 Kitaev systems Na_2IrO_3 , Li_2IrO_3 , $RuCl_3$, and $RuBr_3$ [39, 40], as well as iridium-based mixed-valence hexagonal perovskites [41] by including trigonal distortions [42] on a single-site description of the octahedral environment of the transition-metal d states and derived a modified Curie-Weiss formula in terms of a temperature-dependent magnetic moment. Whereas the temperature dependence of the average magnetic moment in the above d^5 Kitaev systems is not affected by

* yingli1227@xjtu.edu.cn

† valenti@itp.uni-frankfurt.de

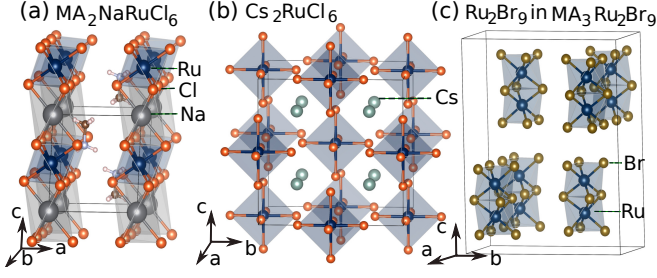


FIG. 2. Crystal structure of (a) $\text{MA}_2\text{NaRuCl}_6$ (b) Cs_2RuCl_6 and (c) Ru_2Br_9 face-shared bioctahedral dimer in $\text{MA}_3\text{Ru}_2\text{Br}_9$.

small trigonal distortions and follows the Kotani model, the components of the magnetic moments do not follow the Kotani formula [39, 40]. For the $4d$ - and $5d$ -based mixed-valence systems with dimerized structures, the Kotani expression fails completely to reproduce their temperature-dependent magnetism [41]. The question is therefore, why does the Kotani formula describe quite accurately the temperature dependence of the magnetic susceptibility and magnetic moments in some spin-orbit coupled systems and it does not for others?

In the present work we uncover the origin of this discrepancy. Specifically we resolve i) the role of electronic fillings shown in Fig. 1 (b), ii) the sensitivity of the magnetic moment components to the crystal-field distortions, iii) the role of Hund's coupling J_H , specially in d^2 systems, iv) the role of intersite hoppings and interactions in dimer systems, and v) the role of $t_{2g} - e_g$ crystal fields [43]. For this purpose, we investigate the magnetic behavior of a few representative systems including $\text{MA}_2\text{NaRuCl}_6$ (d^5), $\text{MA}_3\text{Ru}_2\text{Br}_9$ (d^5), Cs_2RuCl_6 (d^4), and A_2WCl_6 (d^2) by performing exact diagonalization of *ab initio*-derived relativistic multiorbital Hubbard models on finite clusters, computing their magnetic susceptibilities and extracting general rules for the validity range of the Kotani model.

Methods.- To analyze the systems' magnetism we consider the improved Curie-Weiss expression for the diagonal components of the susceptibility [39],

$$\chi^\alpha(T) \approx \chi_0^\alpha + \frac{N_A [m_{\text{eff}}^\alpha(T)]^2}{3k_B(T - \Theta^\alpha)}, \quad (1)$$

where α , T , and χ_0^α indicate the field direction, temperature, and temperature-independent background contributions, respectively. N_A , k_B and Θ^α are Avogadro, Boltzmann and Weiss constants, respectively. m_{eff} denotes the effective magnetic moment. In systems with weak inter-site interactions, the experimentally measured susceptibility is usually mapped to a magnetic moment

$$\tilde{m}_{\text{eff}}^\alpha(T) \approx \sqrt{\frac{3k_B T}{N_A}} \chi^\alpha(T). \quad (2)$$

Here, we denote $\tilde{m}_{\text{eff}}^\alpha(T) = m_{\text{eff}}^\alpha(T)$ only when inter-site hoppings, χ_0 , and Θ^α are set to zero. In our microscopic

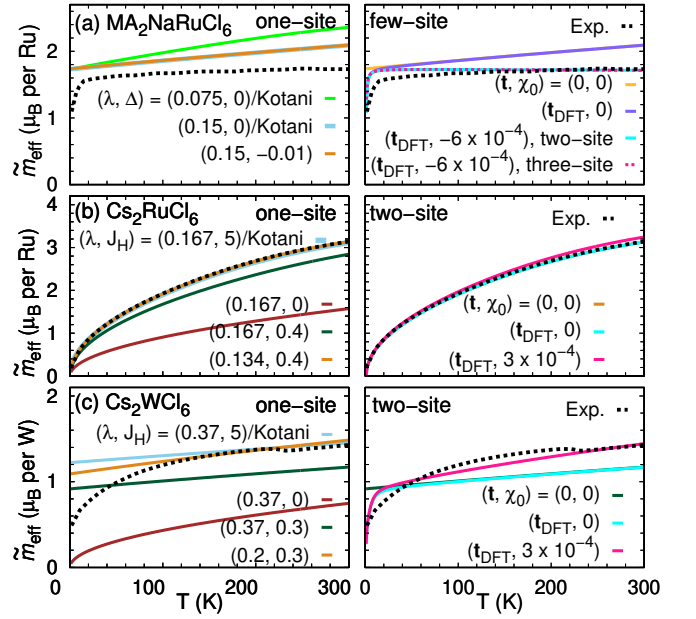


FIG. 3. Temperature dependence of the average magnetic moments for (a) $\text{MA}_2\text{NaRuCl}_6$ (d^5) (b) Cs_2RuCl_6 (d^4) and (c) Cs_2WCl_6 (d^2) from one-site, two-site, and three-sites cluster calculations with various spin-orbit coupling λ , trigonal crystal-fields Δ , Hund's couplings J_H , and hopping parameters \mathbf{t} in eV as well as χ_0 in emu per mol.

approach, we use Eq. 2 [39, 41] to obtain the magnetic moments where the susceptibility is calculated from:

$$\chi^\alpha(T) = \chi_0 + N_A k_B T \left(\frac{1}{Z} \frac{\partial^2 Z}{\partial H_\alpha \partial H_\alpha} \right). \quad (3)$$

H is the external magnetic field and Z is the partition function $Z = \sum_n e^{-E_n/k_B T}$ with E_n being the eigenenergies obtained from exact diagonalization on finite clusters of the Hamiltonian \mathcal{H}_{tot} including the kinetic hopping term (\mathcal{H}_{hop}), crystal-field splitting (\mathcal{H}_{CF}), spin-orbit coupling (\mathcal{H}_{SO}), and Coulomb interaction (\mathcal{H}_U) (see Suppl. Material). The corresponding parameters are hopping parameters \mathbf{t} , crystal-field parameters (Δ), spin-orbit coupling parameter λ , Coulomb repulsion U , and Hund's coupling J_H . \mathbf{t} and Δ were extracted using the Wannier function projection formalism [44–46] from the electronic structure of density functional theory with the full-potential-linearized-augmented-plane-wave basis(LAPW) [47] (see Suppl. Material).

Results.- The dominant crystal information and hopping parameters (summarized in Table I) are discussed here and the details are in the Supplemental Material. Due to the octahedral environment, the transition-metal d states split into e_g and t_{2g} states. We first consider the t_{2g} -only model widely used in these systems.

We start with a d^5 system $\text{MA}_2\text{NaRuCl}_6$ which crystallizes in the space group $P\bar{3}m$ and contains chains of face-sharing RuCl_6 and NaCl_6 octahedra along c [Fig. S1 (a)]. In order to explain the experimentally observed ef-

TABLE I. Largest hopping parameters in meV extracted from DFT calculations for d^5 ($\text{MA}_2\text{NaRuCl}_6$, $\text{MA}_3\text{Ru}_2\text{Br}_9$), d^4 (Cs_2RuCl_6) and d^2 (Cs_2WCl_6) systems.

$\text{MA}_2\text{NaRuCl}_6$	$\text{MA}_3\text{Ru}_2\text{Br}_9$	Cs_2RuCl_6	Cs_2WCl_6
-39.1	-338.6	-38.4	-46.6

fective magnetic moment for $\text{MA}_2\text{NaRuCl}_6$ [29], which deviates from the ideal Kotani model [30], we apply the method described above to single-site, two-site and three-site Ru clusters. We used $U = 2.49$ eV and $J_H = 0.4$ eV following the cRPA values of $\alpha\text{-RuCl}_3$ [40]. The results for \tilde{m}_{eff} are shown in Fig. 3 (a). $\tilde{m}_{\text{eff}} = m_{\text{eff}}$ for the one-site case while $\tilde{m}_{\text{eff}} \neq m_{\text{eff}}$ for the few-sites case with nonzero \mathbf{t} and χ_0 . We observe that the experimental results [29] show lower values of the effective magnetic moment in comparison with the ideal Kotani behavior ($\lambda = 0.075$ eV), and the slopes at low and high temperatures do not fit either. Increasing the value of λ to 0.15 eV, which is comparable to values for other Ru-based systems like $\alpha\text{-RuCl}_3$, reduces the slope of the calculated magnetic moment towards the experimental slope. Including the effect of the trigonal crystal-field distortion $\Delta = -0.01$ eV does not affect the average magnetic moment, but strongly affects the direction-dependent magnetic moments (see Supplemental Material).

Including the contribution of all hopping parameters in the two-site calculation ($\mathbf{t} = \mathbf{t}_{\text{DFT}}$) introduces a sharp reduction of the susceptibility at low temperatures. Actually, the experimentally measured susceptibility also includes a temperature-independent weak contribution χ_0 , originating from core diamagnetism and Van-Vleck paramagnetism [48, 49]. With $\chi_0 = -6 \times 10^{-4}$ emu/mol the effective magnetic moment becomes flat for a range of temperatures between 30 K and 300 K, close to the experimental magnetic moment. We conclude that the deviation of the experimental magnetic moment from the Kotani plot in d^5 system can be attributed to both (i) a temperature-independent χ_0 and (ii) inter-site interactions. Results for two-site and three-site clusters are very close so that we only consider two-site clusters in the following cases.

We now proceed with the d^4 case. The $4d$ -based hybrid vacancy-ordered double perovskite Cs_2RuCl_6 crystallizes in the $Fm\bar{3}m$ space group and consists of isolated RuCl_6 octahedra bound electrostatically by Cs cations [see Fig. S1 (b)]. The largest hopping parameters is -38.4 meV. The results are displayed in Fig. 3 (b). The Kotani plot can be reproduced by considering large unphysical J_H (around 5 eV) with $\lambda = 0.167$ eV, or, alternatively choosing $\lambda = 0.134$ eV, $J_H = 0.4$ eV. In fact, various combination of J_H and λ could reproduce the experimental observations. We also performed two-site cluster calculations with $J_H = 0.4$ eV and find that including χ_0 and hopping parameters modify only slightly the results.

In contrast to d^4 systems, d^2 systems, such as

Cs_2WCl_6 , with similar crystal structures to Cs_2RuCl_6 by replacing Ru with W, display a different behavior. We used $U = 1.7$ eV following values previously used for Ir-based systems [50]. The results are shown in Fig. 3 (c). The Kotani plot with $\lambda \sim 0.37$ eV [38] can only reproduce the slope of the experimental data by considering large unphysical J_H (around 5 eV) where the triplet state is then the ground state in Kotani's perturbation theory. For $J_H = 0$, the ground state is the singlet state with zero magnetic moment at 0 K. In $5d$ systems usual values of J_H are around 0.3 eV [50], and the ground state is a mixing of triplet and singlet states. The magnetic moment is therefore between the above two limits. When decreasing λ to 0.2 eV, the contribution of the triplet states becomes larger, leading to larger magnitudes of the magnetic moments. The two tuning parameters for the magnetic moments are therefore Hund's and spin-orbit coupling strengths. However, different from the d^4 case, the Kotani plot cannot reproduce the experimental data with a combination of λ when assuming physically reasonable values of $J_H = 0.3$ eV. For two-site clusters, the magnitude of the effective magnetic moment is sharply reduced at low temperatures when $\mathbf{t} = \mathbf{t}_{\text{DFT}}$. Including a positive χ_0 brings a downturn in the magnetic moments, close to the experiment. Our method also reproduces the experimental observations for other d^2 systems Rb_2WCl_6 and MA_2WCl_6 (see the Suppl. Material). We conclude that in d^2 systems, besides the contributions of χ_0 and intersite interactions, as in the d^5 systems, the Hund's coupling plays an important role in reproducing the experimental magnetic moments. Finally, for d^1 systems, inclusion of \mathbf{t}_{DFT} , does not affect \tilde{m}_{eff} while adding a nonzero χ_0 significantly changes the slope [see Fig. 4 (a)].

Analyzing the previous results we observe several facts. Already at the level of the Kotani model, the dependence of \tilde{m}_{eff} on the electron filling is rather remarkable, as shown in Fig. 1 (a). For t_{2g} states with spin-orbit coupling, the ground state is more conveniently described in terms of the doublet $j_{1/2}$ and quadruplet $j_{3/2}$ [Fig. 1 (b)]. Different from the atomic relativistic basis j for p orbitals with $L_p = 1$, here $j_{1/2}$ and $j_{3/2}$ correspond to $L_{\text{eff}} = -L_p$. With an electron filling of d^5 , $m_{\text{eff}} = 1.73 \mu_B$ at 0 K which corresponds to one hole in the relativistic $j_{1/2}$ basis, while with an electron filling of d^2 , $m_{\text{eff}} = 1.22 \mu_B$ at 0 K corresponds to a triplet state (in reality there is a reduction of this value due to mixing with a singlet state). For these two cases, inclusion of small intersite hoppings significantly reduces \tilde{m}_{eff} at low temperatures, as demonstrated above.

In contrast, at electron fillings of d^1 and d^4 , intersite hoppings seem to not affect the effective magnetic moments. At these fillings, the Kotani model predicts $m_{\text{eff}} = 0$ at 0 K. These two cases are affected differently by χ_0 . For d^4 systems, the effective magnetic moment changes sharply at values below $k_B T / \lambda \sim 0.2$ and is less influenced by other interactions while the curves for d^1 (also all other fillings) have a smaller slope and are more sen-

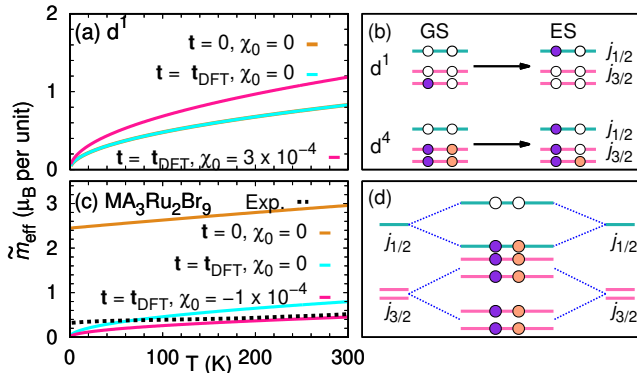


FIG. 4. The average magnetic moments for (a) d^1 system and (c) dimer system $\text{MA}_3\text{Ru}_2\text{Br}_9$ with two-site cluster calculations. Schematic diagrams of (b) ground states and first excited states for d^1 and d^4 systems, as well as (d) the ground state of the dimer system $\text{MA}_3\text{Ru}_2\text{Br}_9$.

sitive to the consideration of further interactions. This could be explained by analyzing the role of the excited states [see Fig. 4 (b)]. In d^1 , there are only two energy levels, the quadruple degenerate ground state $j_{3/2}$ and the doubly degenerate excited state $j_{1/2}$ (magnetic moment $1.73 \mu_B$), the energy difference is $3\lambda/2 \sim 0.22$ eV ($\lambda = 0.15$ eV). At high temperatures, the spin and orbital degrees of freedom are not coupled, therefore the total magnetic moment is $\sqrt{l(l+1) + 4s(s+1)} = \sqrt{5}$ ($s = \frac{1}{2}, l = 1$). The magnetic moment changes slowly from 0 to values around $\sqrt{5}$. In d^4 , the energy difference of the ground state and first excited state is $-\frac{1}{2}(5J_H - \sqrt{25J_H^2 + 10J_H\lambda + 9\lambda^2}) \sim 0.096$ eV ($\lambda \sim 0.15$ eV, $J_H \sim 0.4$ eV). There are more available energy levels and the highest magnetic moment at high temperatures is $\sqrt{10}$ ($s = 1, l = 1$). Therefore, the magnetic moment increases dramatically from 0 to $\sqrt{10}$ in a small temperature region. For d^3 systems, the effective magnetic moment is constant in the Kotani's plot [see Fig. 1 (a)] because the orbital moment is quenched. However, with increasing spin-orbit coupling, in the j_{eff} basis, the total magnetic moment reduces at lower temperatures. This reduction has been observed experimentally in NaOsO_3 [51] and SrTcO_3 [52], and theoretical investigated in Ref. [53].

All systems considered so far have weak inter-site hoppings below 65 meV. In what follows we consider d^5 $\text{MA}_3\text{Ru}_2\text{Br}_9$ which is formed by Ru_2Br_9 dimers comprising two face-sharing RuBr_6 octahedra [see Fig. S1 (c)]. The largest nearest neighbor intra-dimer hopping is -338.6 meV. In order to explain the experimental observed effective magnetic moment, which shows a dramatically low, temperature-independent moment compared to the predicted Kotani behavior, we calculate the temperature-dependent magnetic moments using two-site clusters shown in Fig. 4 (c). Including the intra-dimer hopping parameters, the strong binding splits the single site relativistic $j_{1/2}$ and $j_{3/2}$ basis to form molec-

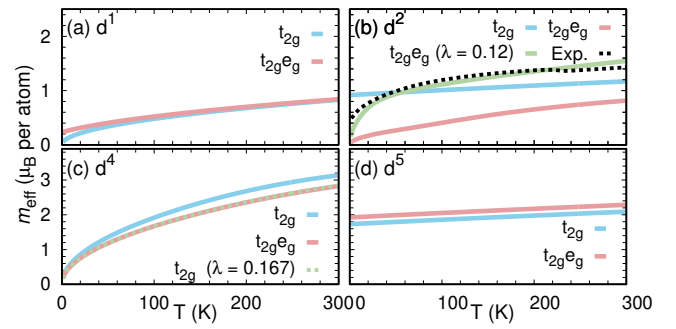


FIG. 5. Temperature dependence of the average magnetic moment for (a) d^1 (b) d^2 (c) d^4 and (d) d^5 including t_{2g} and e_g orbitals.

ular bonding and antibonding energy levels [see Fig. 4 (d)]. The ten electrons and two holes form a singlet $j_{\text{dim}} = 0$ state, similar to the case of $\text{Ba}_3\text{CeIr}_2\text{O}_9$ [54], leading to a significant reduction of the magnetic moments as shown in Fig. 4 (c). Different from experiment, the magnetic moments approach zero at 0 K. These deviations have been suggested to originate from the intra- versus inter-dimer interactions in d^4 systems $\text{Ba}_3\text{ZnIr}_2\text{O}_9$ [55], $\text{Ba}_3\text{CdIr}_2\text{O}_9$ [56], and $\text{Ba}_3\text{MgIr}_2\text{O}_9$ [57]. In our case, inter-dimer interactions and possible impurity effects are not included in our calculations.

From the above results, we observe that in a t_{2g} -only model, the magnetic moments for single site are determined by i) the ground state at 0 K and ii) the energy of the excited states. We now discuss whether including the e_g orbitals suggested in Ref. [43, 58] affect these two factors. The results are displayed in Fig. 5 for various fillings (d^1 , d^2 , d^4 , and d^5) with t_{2g} - e_g crystal fields around 3 eV. For d^1 systems [Fig. 5 (a)], we find that consideration of e_g states induces a non-zero magnetic moment at 0 K of the order of $0.2 \mu_B$, similar to the experimental value for Cs_2TaCl_6 and Rb_2TaCl_6 [59]. In our calculations the small magnetic moments originate from non-zero $j_{1/2}$ states arising from matrix elements between e_g and t_{2g} states. For d^2 systems [Fig. 5 (b)] as in Cs_2WCl_6 , inclusion of e_g states splits the five degenerate d states to a doublet ground states and triplet excited states, strongly reducing the magnetic moment at 0 K [red curve in Fig. 5 (b)]. The energy difference between doublet and triplet is 0.03 eV. By decreasing λ to 0.12 eV, the energy of the first excited states is reduced and the magnetic moment increases dramatically [green curve in Fig. 5 (b)], similar to the experimental observations. Different from Ref. [43], where only the Kanamori model and the first excited state energy gap were used to calculate the susceptibility, our model includes full Coulomb interaction matrices with all Slater parameters as well as all excited states. For d^4 and d^5 fillings, inclusion of e_g states changes minimally the temperature dependence of the magnetic moments.

Conclusions.- Summarizing, we investigated the mag-

netic behavior of a few representative systems including $\text{MA}_2\text{NaRuCl}_6$ (d^5), $\text{MA}_3\text{Ru}_2\text{Br}_9$ (d^5), Cs_2RuCl_6 (d^4), and A_2WCl_6 (d^2) by performing exact diagonalization of *ab initio*-derived relativistic multiorbital Hubbard models on finite clusters. We computed their magnetic susceptibilities and extracted general rules for the validity range of the Kotani model. We find that the slope of the effective magnetic moment is crucially dependent on the ground and excited state configurations at the various electronic fillings. In the single-site description, crystal field distortions, spin-orbit coupling, Hund's coupling, t_{2g-e_g} orbitals, and χ_0 , all contribute to the temperature dependence of the effective magnetic moment in a delicate balance, depending on the electronic filling. While the Kotani model contains contribution of spin-orbit coupling and Hund's coupling, often non-physical values need to be considered to find an agreement with experiment. Furthermore, for systems with strong intradimer interactions, such as $\text{MA}_3\text{Ru}_2\text{Br}_9$, m_{eff} is strongly reduced due to metal-metal bonding.

Our findings resolve the discrepancies between experi-

mental observations and theoretical descriptions of magnetic susceptibilities and effective magnetic moments in spin-orbit-coupled transition metal complexes, and provide a more accurate way to understand magnetism in these systems.

Acknowledgements We thank T. Saha-Dasgupta and A. Paramakanti for discussions. Y.L. acknowledges support by the National Natural Science Foundation of China (Grant No. 12004296), the Fundamental Research Funds for the Central Universities (Grant No. xzy012023051), and HPC Platform, Xi'an Jiaotong University. R.V. acknowledges support by the Deutsche Forschungsgemeinschaft (DFG, German Research Foundation) for funding through Project No. TRR 288 — 422213477 (project A05, B05). R.V.'s research was supported in part by grant NSF PHY-2309135 to the Kavli Institute for Theoretical Physics (KITP). R.S. and S.D.W. thank the NSF Q-AMASE-i Quantum Foundry (DMR-1906325) for support. S.D.W. acknowledges support by DOE, Office of Science, Basic Energy Sciences under Award No. DE-SC0017752. A.K.C. thanks the Ras al Khaimah Centre for Advanced Materials for financial support.

-
- [1] B. Normand, Frontiers in frustrated magnetism, *Contemporary Physics* **50**, 533 (2009).
- [2] L. Balents, Spin liquids in frustrated magnets, *Nature* **464**, 199 (2010).
- [3] Y. Zhou, K. Kanoda, and T.-K. Ng, Quantum spin liquid states, *Rev. Mod. Phys.* **89**, 025003 (2017).
- [4] L. Savary and L. Balents, Quantum spin liquids: a review, *Reports on Progress in Physics* **80**, 016502 (2016).
- [5] C. Broholm, R. J. Cava, S. A. Kivelson, D. G. Nocera, M. R. Norman, and T. Senthil, Quantum spin liquids, *Science* **367**, eaay0668 (2020).
- [6] A. Kitaev, Anyons in an exactly solved model and beyond, *Annals of Physics* **321**, 2 (2006).
- [7] G. Jackeli and G. Khaliullin, Mott insulators in the strong spin-orbit coupling limit: From Heisenberg to a quantum compass and Kitaev models, *Phys. Rev. Lett.* **102**, 017205 (2009).
- [8] J. Chaloupka, G. Jackeli, and G. Khaliullin, Zigzag magnetic order in the iridium oxide Na_2IrO_3 , *Phys. Rev. Lett.* **110**, 097204 (2013).
- [9] W. Witczak-Krempa, G. Chen, Y. B. Kim, and L. Balents, Correlated quantum phenomena in the strong spin-orbit regime, *Annual Review of Condensed Matter Physics* **5**, 57 (2014).
- [10] J. G. Rau, E. K.-H. Lee, and H.-Y. Kee, Spin-orbit physics giving rise to novel phases in correlated systems: Iridates and related materials, *Annual Review of Condensed Matter Physics* **7**, 195 (2016).
- [11] R. Schaffer, E. K.-H. Lee, B.-J. Yang, and Y. B. Kim, Recent progress on correlated electron systems with strong spin-orbit coupling, *Rep. Prog. Phys.* **79**, 094504 (2016).
- [12] S. M. Winter, A. A. Tsirlin, M. Daghofer, J. van den Brink, Y. Singh, P. Gegenwart, and R. Valentí, Models and materials for generalized Kitaev magnetism, *Journal of Physics: Condensed Matter* **29**, 493002 (2017).
- [13] G. Cao and P. Schlottmann, The challenge of spin-orbit-tuned ground states in iridates: a key issues review, *Rep. Prog. Phys.* **81**, 042502 (2018).
- [14] D. A. S. Kaib, S. M. Winter, and R. Valentí, Kitaev honeycomb models in magnetic fields: Dynamical response and dual models, *Phys. Rev. B* **100**, 144445 (2019).
- [15] H. Takagi, T. Takayama, G. Jackeli, G. Khaliullin, and S. E. Nagler, Concept and realization of Kitaev quantum spin liquids, *Nature Reviews Physics* **1**, 264 (2019).
- [16] S. Trebst and C. Hickey, Kitaev materials, *Physics Reports* **950**, 1 (2022).
- [17] M. Hermanns, I. Kimchi, and J. Knolle, Physics of the Kitaev model: Fractionalization, dynamic correlations, and material connections, *Annual Review of Condensed Matter Physics* **9**, 17 (2018).
- [18] L. E. Chern and Y. B. Kim, Magnetic order with fractionalized excitations in pyrochlore magnets with strong spin-orbit coupling, *Scientific Reports* **9**, 10974 (2019).
- [19] J. Knolle, D. L. Kovrizhin, J. T. Chalker, and R. Moessner, Dynamics of fractionalization in quantum spin liquids, *Phys. Rev. B* **92**, 115127 (2015).
- [20] G. Chen, R. Pereira, and L. Balents, Exotic phases induced by strong spin-orbit coupling in ordered double perovskites, *Phys. Rev. B* **82**, 174440 (2010).
- [21] A. S. Erickson, S. Misra, G. J. Miller, R. R. Gupta, Z. Schlesinger, W. A. Harrison, J. M. Kim, and I. R. Fisher, Ferromagnetism in the mott insulator $\text{Ba}_2\text{NaOsO}_6$, *Phys. Rev. Lett.* **99**, 016404 (2007).
- [22] L. Lu, M. Song, W. Liu, A. P. Reyes, P. Kuhns, H. O. Lee, I. R. Fisher, and V. F. Mitrović, Magnetism and local symmetry breaking in a mott insulator with strong spin orbit interactions, *Nature Communications* **8**, 14407 (2017).
- [23] D. Hirai, H. Sagayama, S. Gao, H. Ohsumi, G. Chen, T.-h. Arima, and Z. Hiroi, Detection of multipolar orders

- in the spin-orbit-coupled $5d$ mott insulator $\text{Ba}_2\text{MgReO}_6$, *Phys. Rev. Res.* **2**, 022063 (2020).
- [24] F. I. Frontini, G. H. J. Johnstone, N. Iwahara, P. Bhattacharyya, N. A. Bogdanov, L. Hozoi, M. H. Upton, D. M. Casa, D. Hirai, and Y.-J. Kim, Spin-orbit-lattice entangled state in a_2mgreo_6 ($A = \text{Ca, sr, ba}$) revealed by resonant inelastic x-ray scattering, *Phys. Rev. Lett.* **133**, 036501 (2024).
- [25] A. Kojima, K. Teshima, Y. Shirai, and T. Miyasaka, Organometal halide perovskites as visible-light sensitizers for photovoltaic cells, *Journal of the American Chemical Society* **131**, 6050 (2009).
- [26] M. A. Green, A. Ho-Baillie, and H. J. Snaith, The emergence of perovskite solar cells, *Nature Photonics* **8**, 506 (2014).
- [27] J. Burschka, N. Pellet, S.-J. Moon, R. Humphry-Baker, P. Gao, M. K. Nazeeruddin, and M. Grätzel, Sequential deposition as a route to high-performance perovskite-sensitized solar cells, *Nature* **499**, 316 (2013).
- [28] J.-H. Im, I.-H. Jang, N. Pellet, M. Grätzel, and N.-G. Park, Growth of $\text{CH}_3\text{NH}_3\text{PbI}_3$ cuboids with controlled size for high-efficiency perovskite solar cells, *Nature Nanotechnology* **9**, 927 (2014).
- [29] P. Vishnoi, J. L. Zuo, T. A. Strom, G. Wu, S. D. Wilson, R. Seshadri, and A. K. Cheetham, Structural diversity and magnetic properties of hybrid ruthenium halide perovskites and related compounds, *Angewandte Chemie International Edition* **59**, 8974 (2020).
- [30] M. Kotani, On the magnetic moment of complex ions. (i), *Journal of the Physical Society of Japan* **4**, 293 (1949).
- [31] R. B. Johannesen and G. A. Candela, Magnetic susceptibilities and dilution effects in low-spin d^4 complexes: Osmium(IV), *Inorg. Chem.* **2**, 67 (1963).
- [32] A. Earnshaw, B. N. Figgis, J. Lewis, and R. D. Peacock, 601. the magnetic properties of some d^4 -complexes, *J. Chem. Soc.*, 3132 (1961).
- [33] P. Vishnoi, J. L. Zuo, J. A. Cooley, L. Kautzsch, A. Gómez-Torres, J. Murillo, S. Fortier, S. D. Wilson, R. Seshadri, and A. K. Cheetham, Chemical control of spin-orbit coupling and charge transfer in vacancy-ordered ruthenium(IV) halide perovskites, *Angewandte Chemie International Edition* **60**, 5184.
- [34] H. Lu, J. R. Chamorro, C. Wan, and T. M. McQueen, Universal single-ion physics in spin-orbit-coupled d^5 and d^4 ions, *Inorg. Chem.* **57**, 14443 (2018).
- [35] D. Appleby, P. B. Hitchcock, K. R. Seddon, J. E. Turp, J. A. Zora, C. L. Hussey, J. R. Sanders, and T. A. Ryan, Tri- μ -bromo-bis[tribromoruthenate(III)] salts: a synthetic, structural, spectroscopic, and electrochemical study, *J. Chem. Soc., Dalton Trans.*, 1879 (1990).
- [36] C. D. Kennedy and R. D. Peacock, 629. complex chlorides and bromides of quadrivalent tungsten, *J. Chem. Soc.*, 3392 (1963).
- [37] Z. Liu, X. Qin, Q. Chen, Q. Chen, Y. Jing, Z. Zhou, Y. S. Zhao, J. Chen, and X. Liu, Highly stable lead-free perovskite single crystals with NIR emission beyond 1100 nm, *Advanced Optical Materials* **10**, 2201254.
- [38] E. E. Morgan, G. T. Kent, A. Zohar, A. O’Dea, G. Wu, A. K. Cheetham, and R. Seshadri, Hybrid and inorganic vacancy-ordered double perovskites A_2WCl_6 , *Chem. Mater.* **35**, 7032 (2023).
- [39] Y. Li, S. M. Winter, D. A. S. Kaib, K. Riedl, and R. Valentí, Modified curie-weiss law for j_{eff} magnets, *Phys. Rev. B* **103**, L220408 (2021).
- [40] D. A. S. Kaib, K. Riedl, A. Razpopov, Y. Li, S. Backes, I. I. Mazin, and R. Valentí, Electronic and magnetic properties of the RuX_3 ($X = \text{Cl, Br, I}$) family: two siblings—and a cousin?, *npj Quantum Materials* **7**, 75 (2022).
- [41] Y. Li, A. A. Tsirlin, T. Dey, P. Gegenwart, R. Valentí, and S. M. Winter, Soft and anisotropic local moments in $4d$ and $5d$ mixed-valence M_2O_9 dimers, *Phys. Rev. B* **102**, 235142 (2020).
- [42] H. Kamimura, On the Magnetic Moment and g-Value of Complex Ions, *J. Phys. Soc. Jpn.* **11**, 1171 (1956).
- [43] K. Pradhan, A. Paramekanti, and T. Saha-Dasgupta, Multipolar magnetism in $5d^2$ vacancy-ordered halide double perovskites, *Phys. Rev. B* **109**, 184416 (2024).
- [44] M. Aichhorn, L. Pourovskii, V. Vildosola, M. Ferrero, O. Parcollet, T. Miyake, A. Georges, and S. Biermann, Dynamical mean-field theory within an augmented plane-wave framework: Assessing electronic correlations in the iron pnictide LaFeAsO , *Physical Review B* **80**, 085101 (2009).
- [45] K. Foyevtsova, H. O. Jeschke, I. I. Mazin, D. I. Khomskii, and R. Valentí, Ab initio analysis of the tight-binding parameters and magnetic interactions in na_2iro_3 , *Phys. Rev. B* **88**, 035107 (2013).
- [46] J. Ferber, K. Foyevtsova, H. O. Jeschke, and R. Valentí, Unveiling the microscopic nature of correlated organic conductors: The case of κ -(ET) $_2\text{Cu}[\text{N}(\text{CN})_2]\text{Br}_x\text{Cl}_{1-x}$, *Physical Review B* **89**, 205106 (2014).
- [47] P. Blaha, K. Schwarz, F. Tran, R. Laskowski, G. K. H. Madsen, and L. D. Marks, Wien2k: An apw+lo program for calculating the properties of solids, *The Journal of Chemical Physics* **152**, 074101 (2020).
- [48] A. Nag and S. Ray, Misjudging frustrations in spin liquids from oversimplified use of curie-weiss law, *Journal of Magnetism and Magnetic Materials* **424**, 93 (2017).
- [49] H. B. Bebb and A. Gold, Multiphoton ionization of hydrogen and rare-gas atoms, *Phys. Rev.* **143**, 1 (1966).
- [50] S. M. Winter, Y. Li, H. O. Jeschke, and R. Valentí, Challenges in design of Kitaev materials: Magnetic interactions from competing energy scales, *Phys. Rev. B* **93**, 214431 (2016).
- [51] Y. G. Shi, Y. F. Guo, S. Yu, M. Arai, A. A. Belik, A. Sato, K. Yamaura, E. Takayama-Muromachi, H. F. Tian, H. X. Yang, J. Q. Li, T. Varga, J. F. Mitchell, and S. Okamoto, Continuous metal-insulator transition of the antiferromagnetic perovskite NaOsO_3 , *Phys. Rev. B* **80**, 161104 (2009).
- [52] E. E. Rodriguez, F. Poineau, A. Llobet, B. J. Kennedy, M. Avdeev, G. J. Thorogood, M. L. Carter, R. Seshadri, D. J. Singh, and A. K. Cheetham, High temperature magnetic ordering in the $4d$ perovskite SrTcO_3 , *Phys. Rev. Lett.* **106**, 067201 (2011).
- [53] H. Matsuura and K. Miyake, Effect of spin-orbit interaction on $(4d)3-$ and $(5d)3-$ -based transition-metal oxides, *Journal of the Physical Society of Japan* **82**, 073703 (2013).
- [54] A. Revelli, M. M. Sala, G. Monaco, P. Becker, L. Bohatý, M. Hermanns, T. C. Koethe, T. Fröhlich, P. Warzanowski, T. Lorenz, S. V. Streltsov, P. H. M. van Loosdrecht, D. I. Khomskii, J. van den Brink, and M. Grüninger, Resonant inelastic x-ray incarnation of young’s double-slit experiment, *Science Advances* **5**, eaav4020 (2019).
- [55] A. Nag, S. Middey, S. Bhowal, S. K. Panda, R. Math-

- ieu, J. C. Orain, F. Bert, P. Mendels, P. G. Freeman, M. Mansson, H. M. Ronnow, M. Telling, P. K. Biswas, D. Sheptyakov, S. D. Kaushik, V. Siruguri, C. Meneghini, D. D. Sarma, I. Dasgupta, and S. Ray, Origin of the spin-orbital liquid state in a nearly $j = 0$ iridate $\text{Ba}_3\text{ZnIr}_2\text{O}_9$, *Phys. Rev. Lett.* **116**, 097205 (2016).
- [56] M. S. Khan, A. Bandyopadhyay, A. Nag, V. Kumar, A. V. Mahajan, and S. Ray, Magnetic ground state of the distorted 6H perovskite $\text{Ba}_3\text{CdIr}_2\text{O}_9$, *Phys. Rev. B* **100**, 064423 (2019).
- [57] A. Nag, S. Bhowal, F. Bert, A. D. Hillier, M. Itoh, I. Carlomagno, C. Meneghini, T. Sarkar, R. Mathieu, I. Dasgupta, and S. Ray, $\text{Ba}_3\text{MnIr}_2\text{O}_9$ hexagonal perovskites in the light of spin-orbit coupling and local structural distortions, *Phys. Rev. B* **97**, 064408 (2018).
- [58] G. L. Stamokostas and G. A. Fiete, Mixing of $t_{2g} - e_g$ orbitals in $4d$ and $5d$ transition metal oxides, *Phys. Rev. B* **97**, 085150 (2018).
- [59] H. Ishikawa, T. Takayama, R. K. Kremer, J. Nuss, R. Dinnebier, K. Kitagawa, K. Ishii, and H. Takagi, Ordering of hidden multipoles in spin-orbit entangled $5d^1$ ta chlorides, *Phys. Rev. B* **100**, 045142 (2019).

Supplemental Material:
Microscopic origin of temperature-dependent magnetism in spin-orbit-coupled transition metal compounds

1. Electronic Hamiltonian

The Coulomb terms in the t_{2g} basis of H_{tot} are given by:

$$\begin{aligned} \mathcal{H}_U &= U \sum_{i,a} n_{a,\uparrow} n_{i,a,\downarrow} + (U' - J_H) \sum_{i,a < b, \sigma} n_{i,a,\sigma} n_{i,b,\sigma} \\ &+ U' \sum_{i,a \neq b} n_{i,a,\uparrow} n_{i,b,\downarrow} - J_H \sum_{i,a \neq b} c_{i,a,\uparrow}^\dagger c_{i,a,\downarrow} c_{i,b,\downarrow}^\dagger c_{i,b,\uparrow} \\ &+ J_H \sum_{i,a \neq b} c_{i,a,\uparrow}^\dagger c_{i,a,\downarrow}^\dagger c_{i,b,\downarrow} c_{i,b,\uparrow}, \end{aligned} \quad (\text{S1})$$

where $c_{i,a}^\dagger$ creates an electron in orbital $a \in \{yz, xz, xy\}$ at site i ; J_H gives the strength of Hund's coupling, U is the *intraorbital* Coulomb repulsion, and $U' = U - 2J_H$ is the *interorbital* repulsion. The one particle terms are most conveniently written in terms of:

$$\vec{c}_i^\dagger = \left(c_{i,yz,\uparrow}^\dagger \ c_{i,yz,\downarrow}^\dagger \ c_{i,xz,\uparrow}^\dagger \ c_{i,xz,\downarrow}^\dagger \ c_{i,xy,\uparrow}^\dagger \ c_{i,xy,\downarrow}^\dagger \right). \quad (\text{S2})$$

Spin-orbit coupling is described by:

$$\mathcal{H}_{\text{SO}} = \frac{\lambda}{2} \sum_i \vec{c}_i^\dagger \begin{pmatrix} 0 & i\sigma_z & -i\sigma_y \\ -i\sigma_z & 0 & i\sigma_x \\ i\sigma_y & -i\sigma_x & 0 \end{pmatrix} \vec{c}_i, \quad (\text{S3})$$

where σ_α , $\alpha = \{x, y, z\}$ are Pauli matrices. Their matrix is used for all materials except $\text{MA}_3\text{Ru}_2\text{Br}_9$, where two Ru atoms have two local coordinates. For convenience, we choose as global spin quantization axis to be the crystallographic c -axis, but employ local coordinates for the orbital definitions. The spin operator are then modified by the rotation from the global coordinates to the local coordinates for the orbital, similar as MO_9 dimers[41]. The crystal-field Hamiltonian is given by:

$$\mathcal{H}_{\text{CF}} = \sum_i \vec{c}_i^\dagger \{ \Delta_i \otimes \mathbb{I}_{2 \times 2} \} \vec{c}_i, \quad (\text{S4})$$

where $\mathbb{I}_{2 \times 2}$ is the 2×2 identity matrix; Δ_i is the crystal field tensor. The hopping Hamiltonian is most generally written:

$$\mathcal{H}_{\text{hop}} = \sum_{ij} \vec{c}_i^\dagger \{ \mathbf{T}_{ij} \otimes \mathbb{I}_{2 \times 2} \} \vec{c}_j, \quad (\text{S5})$$

with the hopping matrices \mathbf{T}_{ij} defined for each bond connecting sites i, j .

Including the e_g for one-site cluster, the Coulomb terms are generally written as:

$$\mathcal{H}_U = \sum_{\alpha, \beta, \delta, \gamma} U_{\alpha\beta\gamma\delta} c_{i,\alpha,\sigma}^\dagger c_{i,\beta,\sigma'}^\dagger c_{i,\gamma,\sigma'} c_{i,\delta,\sigma} \quad (\text{S6})$$

where $\alpha, \beta, \gamma, \delta$ are different d orbital indices [?]. In the spherically symmetric approximation [? ?], the coefficient $U_{\alpha\beta\gamma\delta}$ are all related to the three Slater parameters F_0, F_2, F_4 , which are expressed in terms of Kanamori parameter U and J_H in t_{2g} basis:

$$\begin{aligned} F_0 &= U - \frac{13}{49} \frac{441}{79} J_H \\ F_2 &= \frac{882}{79} J_H, \\ F_4 &= \frac{5}{4} \frac{441}{79} J_H. \end{aligned} \quad (\text{S7})$$

The formula is reduced to Kanamori formula when the number of unique orbital indices are one or two. Beyond the Kanamori formula, the Coulomb coefficients with three and four indices are significant for the small energy gap between ground state and excited states when both e_g and t_{2g} orbitals are included. The spin-orbit coupling is changed to:

$$\mathcal{H}_{\text{SO}} = \frac{\lambda}{2} \sum_i \vec{c}_i^\dagger \begin{pmatrix} 0 & 0 & i\sqrt{3}\sigma_x & -i\sqrt{3}\sigma_y & 0 \\ 0 & 0 & i\sigma_x & i\sigma_y & -2i\sigma_z \\ -i\sqrt{3}\sigma_x & -i\sigma_x & 0 & i\sigma_z & -i\sigma_y \\ i\sqrt{3}\sigma_y & -i\sigma_y & -i\sigma_z & 0 & i\sigma_x \\ 0 & 2i\sigma_z & i\sigma_y & -i\sigma_x & 0 \end{pmatrix} \vec{c}_i, \quad (\text{S8})$$

where the basis \vec{c}_i^\dagger is $(c_{i,z^2,\uparrow}^\dagger \ c_{i,z^2,\downarrow}^\dagger \ c_{i,x^2-y^2,\uparrow}^\dagger \ c_{i,x^2-y^2,\downarrow}^\dagger \ c_{i,yz,\uparrow}^\dagger \ c_{i,yz,\downarrow}^\dagger \ c_{i,xz,\uparrow}^\dagger \ c_{i,xz,\downarrow}^\dagger \ c_{i,xy,\uparrow}^\dagger \ c_{i,xy,\downarrow}^\dagger)$.

2. Hopping parameters from density functional theory

The hopping parameters for the multiorbital Hubbard models were extracted using the Wannier function projection formalism proposed in Ref. [44–46] from the electronic structure of density functional theory with the full-potential-linearized-augmented-plane-wave basis (LAPW) as implemented in WIEN2k [47]. We employed the Perdew-Burke-Ernzerhof generalized gradient approximation [?] as exchange-correlation functional. For the calculations we considered a k-mesh of

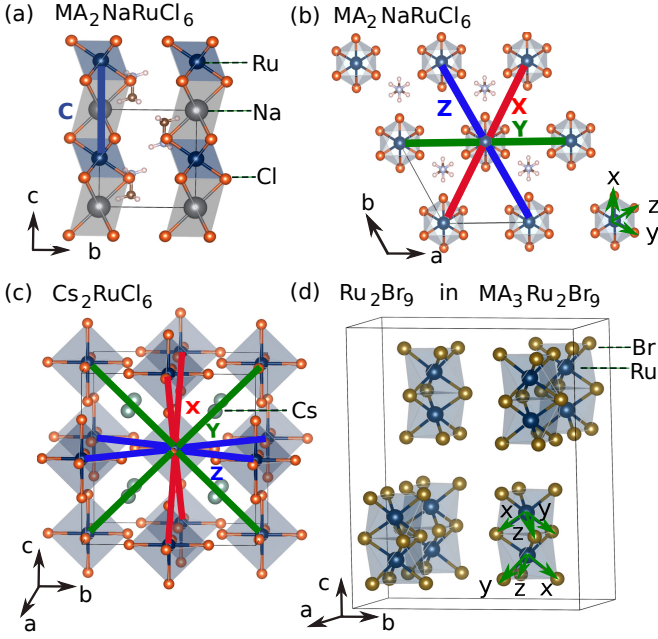


FIG. S1. Crystal structure of $\text{MA}_2\text{NaRuCl}_6$ along (a) bc - and (b) ab -planes. (c) Crystal structure of Cs_2RuCl_6 . The three different types of bonds X , Y , and Z , are shown in red, green and blue, respectively. (d) Ru_2Br_9 face-shared bioctahedral dimer in $\text{MA}_3\text{Ru}_2\text{Br}_9$. Green arrows denote local coordinates.

TABLE SI. Parameters for crystal-field splitting and hopping (meV) in Eq.S9-S15 extracted from DFT calculations for various materials.

$d^5 \text{MA}_2\text{NaRuCl}_6$						
Δ	t_C	t'_C	t_1	t_2	t_3	t_4
-10.0	-4.1	-18.0	2.3	-7.4	-39.1	0.6
$d^5 \text{MA}_3\text{Ru}_2\text{Br}_9$						
Δ_1	Δ_2	Δ_3	t_a	t_b	t'_a	t'_b
-99.0	-48.9	-59.6	-336.4	-338.6	-309.6	-250.1
d^4 and d^2						
	Cs_2RuCl_6	Cs_2WCl_6	Rb_2WCl_6	MA_2WCl_6		
Δ	0	0	0	1.8		
t_1	7.3	11.5	3.9	1.9		
t_2	-8.3	9.6	-9.6	-12.9		
t_3	-46.6	-38.4	-61.4	-62.2		
t_4	0	0	0	0.6		

300 \mathbf{k} points in the first Brillouin zone and the parameter RK_{max} was set to 7 (3) for systems without (with) hydrogens, respectively. We consider first the case of a d^5 system $\text{MA}_2\text{NaRuCl}_6$ in Fig. S1 (a)-(b). We label the nearest-neighbor Ru-Ru bonds along the c axis as C bonds, and as X , Y , Z bonds the next-nearest neighbor Ru-Ru bonds which lie in the ab plane forming a Ru triangular lattice. In the t_{2g} basis, the tetragonal distortion of the octahedron is zero while there is a small

trigonal distortion Δ . In the $4d$ -based hybrid vacancy-ordered double perovskites Cs_2RuCl_6 [see Fig. S1 (c)], each Ru has four nearest neighbor bonds along ac , bc , and ab planes, labeled as X , Y , and Z bonds, respectively. The local coordinates are set to be the same as the global a , b , c axes. Different from Cs_2RuCl_6 and Rb_2WCl_6 , in MA_2WCl_6 , the W form a triangular lattice in the ab plane, similar to $\text{MA}_2\text{NaRuCl}_6$. The crystal field Δ_i for $\text{MA}_2\text{NaRuCl}_6$, MA_2WCl_6 , Cs_2RuCl_6 , and Cs_2WCl_6 are written as:

$$\Delta_i = \begin{pmatrix} 0 & \Delta & \Delta \\ \Delta & 0 & \Delta \\ \Delta & \Delta & 0 \end{pmatrix}, \quad (\text{S9})$$

The hopping integrals for the nearest neighbour C -bond [Fig. S1 (a)] in $\text{MA}_2\text{NaRuCl}_6$ are given by:

$$\mathbf{T}^C = \begin{pmatrix} t_C & t'_C & t'_C \\ t'_C & t_C & t'_C \\ t'_C & t'_C & t_C \end{pmatrix}. \quad (\text{S10})$$

The hopping integrals for the nearest neighbour Z -bond in $\text{MA}_2\text{NaRuCl}_6$, MA_2WCl_6 , Cs_2RuCl_6 , and Cs_2WCl_6 are written as:

$$\mathbf{T}^Z = \begin{pmatrix} t_1 & t_2 & t_4 \\ t_2 & t_1 & t_4 \\ t_4 & t_4 & t_3 \end{pmatrix}. \quad (\text{S11})$$

While X and Y bonds are given by:

$$\mathbf{T}^X = \begin{pmatrix} t_3 & t_4 & t_4 \\ t_4 & t_1 & t_2 \\ t_4 & t_2 & t_1 \end{pmatrix}, \quad (\text{S12})$$

$$\mathbf{T}^Y = \begin{pmatrix} t_1 & t_4 & t_2 \\ t_4 & t_3 & t_4 \\ t_2 & t_4 & t_1 \end{pmatrix}. \quad (\text{S13})$$

For $\text{MA}_3\text{Ru}_2\text{Br}_9$ shown in Fig. S1 (d), the Ru-Ru bond distances are around 2.4 - 2.5 Å, forming Ru-Ru bonding. Different from the case of inorganic compounds including M_2O_9 ($\text{M} = \text{Ir}, \text{Ru}$) dimers [41], where the local D_{3h} point group symmetry within each dimer implies only one onsite trigonal term Δ and two types of hopping integrals: diagonal and off-diagonal in the local M -O x , y , z coordinates, the three Ru-Br bond-lengths in $\text{MA}_3\text{Ru}_2\text{Br}_9$ are different, leading to splittings of the onsite crystal field

$$\Delta_i = \begin{pmatrix} 0 & \Delta_2 & \Delta_1 \\ \Delta_2 & 0 & \Delta_1 \\ \Delta_1 & \Delta_1 & \Delta_3 \end{pmatrix}. \quad (\text{S14})$$

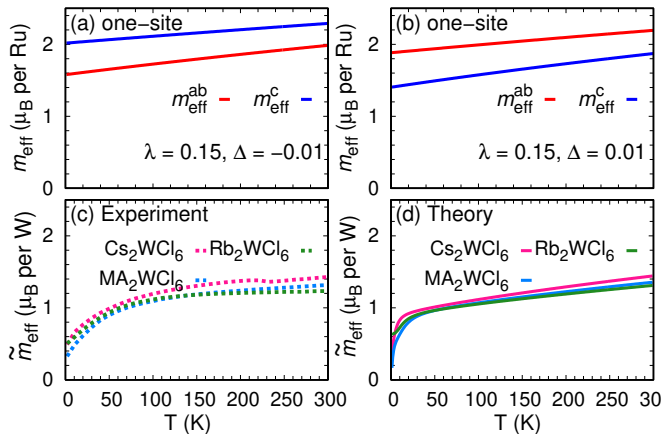


FIG. S2. Temperature dependence of the magnetic moments for in-plane direction (m_{eff}^{ab}) and out-of-plane direction (m_{eff}^c) in d^5 system $\text{MA}_2\text{NaRuCl}_6$ for (a) $\Delta = -0.01$ eV and (b) $\Delta = 0.01$ eV with $\lambda = 0.15$ eV. (c), (d) Comparison of experimental [33, 38] and calculated magnetic moments for Cs_2WCl_6 , Rb_2WCl_6 , and MA_2WCl_6 .

The hopping matrix intra the dimers for $\text{MA}_3\text{Ru}_2\text{Br}_9$ are written as:

$$\mathbf{T} = \begin{pmatrix} t_a & t_b & t'_b \\ t_b & t_a & t'_b \\ t'_b & t'_b & t'_a \end{pmatrix}. \quad (\text{S15})$$

The corresponding hopping parameters are displayed in Table SI.

3. Direction-dependent magnetic moments for d^5 system and average magnetic moments for d^2 materials

Δ strongly affects the direction-dependent magnetic moments m_{eff}^{ab} and m_{eff}^c as shown in Fig. S2 (a) and (b) for $\text{MA}_2\text{NaRuCl}_6$. Our method also reproduces the experimental observations for other d^2 systems Rb_2WCl_6 and MA_2WCl_6 [see Fig. S2 (c), (d)].